Article

Structure

Cdc123, a Cell Cycle Regulator Needed for eIF2 Assembly, Is an ATP-Grasp Protein with Unique Features

Graphical Abstract

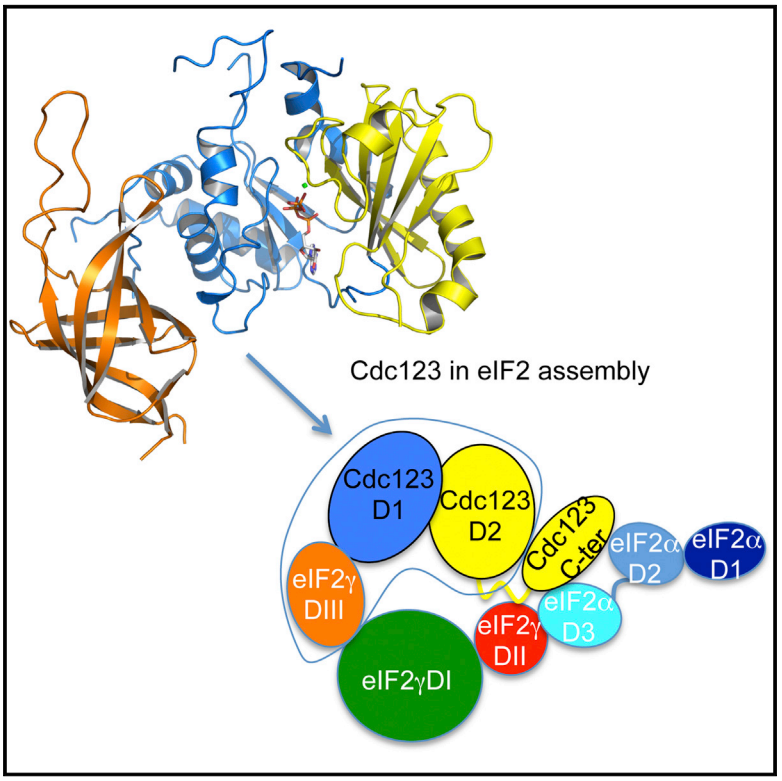

Authors

Michel Panvert, Etienne Dubiez, Lea Arnold, ..., Yves Mechulam, Wolfgang Seufert, Emmanuelle Schmitt

Correspondence

emma@bioc.polytechnique.fr (E.S.), wolfgang.seufert@ur.de (W.S.)

In Brief

Cell proliferation protein Cdc123 participates in the assembly of eIF2 from its three subunits. Cdc123 resembles proteins of the ATP-grasp family. The structure of Cdc123 bound to an eIF2 domain allows Panvert et al. to propose a model explaining how Cdc123 facilitates assembly of eIF2γ to eIF2α.

Highlights

- Cdc123 is an atypical ATP-grasp protein
- ATP binding to Cdc123 is required for eIF2 assembly and cell viability
- A model accounting for the role of Cdc123 in assembly of eIF2γ to eIF2α is proposed

Accession Numbers

4ZGO
4ZGP
4ZGN
4ZGQ

Panvert et al., 2015, Structure *23*, 1596–1608
September 1, 2015
http://dx.doi.org/10.1016/j.str.2015.06.014

CellPress

Structure
Article

Cdc123, a Cell Cycle Regulator Needed for eIF2 Assembly, Is an ATP-Grasp Protein with Unique Features

Michel Panvert,[1] Etienne Dubiez,[1] Lea Arnold,[2] Javier Perez,[3] Yves Mechulam,[1] Wolfgang Seufert,[2,*] and Emmanuelle Schmitt[1,*]
[1]Laboratoire de Biochimie, Ecole Polytechnique, CNRS, UMR7654, 91128 Palaiseau Cedex, France
[2]Department of Genetics, University of Regensburg, 93040 Regensburg, Germany
[3]SOLEIL Synchrotron, L'Orme des Merisiers, 91190 Saint Aubin, France
*Correspondence: emma@bioc.polytechnique.fr (E.S.), wolfgang.seufert@ur.de (W.S.)
http://dx.doi.org/10.1016/j.str.2015.06.014

SUMMARY

Eukaryotic initiation factor 2 (eIF2), a heterotrimeric guanosine triphosphatase, has a central role in protein biosynthesis by supplying methionylated initiator tRNA to the ribosomal translation initiation complex and by serving as a target for translational control in response to stress. Recent work identified a novel step indispensable for eIF2 function: assembly of eIF2 from its three subunits by the cell proliferation protein Cdc123. We report the first crystal structure of a Cdc123 representative, that from *Schizosaccharomyces pombe*, both isolated and bound to domain III of *Saccharomyces cerevisiae* eIF2γ. The structures show that Cdc123 resembles enzymes of the ATP-grasp family. Indeed, Cdc123 binds ATP-Mg^{2+}, and conserved residues contacting ATP-Mg^{2+} are essential for Cdc123 to support eIF2 assembly and cell viability. A docking of eIF2αγ onto Cdc123, combined with genetic and biochemical experiments, allows us to propose a model explaining how Cdc123 participates in the biogenesis of eIF2 through facilitating assembly of eIF2γ to eIF2α.

INTRODUCTION

Initiation of the translation of an mRNA into a protein involves a complex cascade of molecular events, leading to a translation-competent ribosome with a methionylated initiator tRNA in the P site, base-paired with the start codon on mRNA (Hinnebusch, 2011; Lorsch and Dever, 2010). A critical consequence of the whole process is the setting of the reading frame for mRNA decoding. In eukaryotic and archaeal cells, the initiator tRNA carrier is the e/aIF2 heterotrimer. e/aIF2 results from the association of three subunits, α, β, and γ. The γ subunit forms the core of the heterotrimer. It interacts with both α and β subunits while α and β do not interact together (Schmitt et al., 2010). In its guanosine triphosphate (GTP)-bound form, this factor specifically binds Met-$tRNA_i^{Met}$ (Schmitt et al., 2012) and handles it in the initiation complex (Huang et al., 1997). After start codon recognition, the factor, in its guanosine diphosphate-bound form, loses affinity for Met-$tRNA_i^{Met}$ and eventually dissociates from the initiation complex (Algire et al., 2005). This leaves Met-$tRNA_i^{Met}$ in the P site of the small ribosomal subunit and allows the final steps of initiation to occur. In this process, specific handling of the initiator tRNA by e/aIF2 and control of the nucleotide state of the factor are crucial for accuracy.

According to its central role in translation, eIF2 was identified early as a central target in response to stress conditions (Gebauer and Hentze, 2004; Holcik and Sonenberg, 2005). Such conditions trigger phosphorylation of the α subunit of the heterotrimer that, in turn, leads eIF2 to form an inactive complex with the guanine nucleotide exchange factor eIF2B. The subsequent sequestering of eIF2 reprograms gene expression by both reducing global translation and specifically enhancing the translation of mRNAs encoding activators of the transcription of stress adaptation genes (Hinnebusch, 2005).

Proteomic studies in *Saccharomyces cerevisiae* have reported interaction of the γ subunit of eIF2 with the cell proliferation protein Cdc123 (e.g. Ho et al., 2002). This gene was first identified in mammals as the target of mutations blocking the G1-S transition in the cell cycle (Ohno et al., 1984; Okuda and Kimura, 1996). In human, CDC123 was described as a candidate oncogene in breast cancer (Adelaide et al., 2007) and was implicated in other diseases (Soler Artigas et al., 2011; Zeggini et al., 2008). Relationships between eIF2 and Cdc123 became clearer when it was shown that assembly of the eIF2 complex in vivo depended on Cdc123 (Perzlmaier et al., 2013). Indeed, mutations of Cdc123 in budding yeast reduced the association of the eIF2 subunits, diminished polysome levels, and increased *GCN4* expression, indicating that Cdc123 was critical for eIF2 activity. Using co-immunoprecipitation (co-IP) from *S. cerevisiae* cell extracts as well as pull-down experiments with *Escherichia coli* expressed proteins, an interaction between Cdc123 and the unassembled γ subunit of eIF2 was shown (Perzlmaier et al., 2013). More precisely, the results have indicated that domain III of the γ subunit of eIF2 was required for binding to Cdc123. Alterations of the binding site revealed a strict correlation between Cdc123 binding, the biological function of eIF2γ, and its ability to assemble with α and β subunits. Overexpression of Cdc123 neutralized the eIF2 assembly defect. Moreover, overexpression of eIF2 α or γ subunits rescued an otherwise inviable *cdc123*

deletion mutant with a strong synergistic effect when both α and γ subunits were overproduced. In contrast, overexpression of eIF2β could not compensate for the absence of Cdc123. Thus, Cdc123 has appeared as an essential protein acting as a specific assembly factor of the eIF2 heterotrimeric complex by promoting the eIF2αγ assembly step (Perzlmaier et al., 2013). The requirement of Cdc123 in eukaryotes may explain why all attempts to produce isolated yeast eIF2γ were unsuccessful (Naveau et al., 2013).

Here, we report the first crystal structure of a Cdc123 representative, that from *Schizosaccharomyces pombe*, both isolated and bound to the domain III of eIF2γ (γDIII) from *S. cerevisiae*. Cdc123 resembles enzymes of the ATP-grasp family, and indeed binds ATP-Mg^{2+}. Structural data and biochemical studies revealed that ATP-Mg^{2+} is needed for Cdc123 activity. A docking of eIF2αγ onto Cdc123 allows us to propose a tentative model explaining how Cdc123 participates in the biogenesis of eIF2 through facilitating assembly of eIF2γ to eIF2α.

RESULTS

Overall Structure of Sp-Cdc123

Despite many attempts, no crystal could be obtained using Cdc123 from *S. cerevisiae* (Sc-Cdc123). Therefore, we chose to purify Cdc123 from *Schizosaccharomyces pombe*, Sp-Cdc123. Indeed, the two proteins share 35% identities (55% similarities). Moreover, Sp-Cdc123 is shorter than Sc-Cdc123 (319 amino acids compared with 360 in the case of Sc-Cdc123) with smaller predicted loop regions (Cole et al., 2008; Figure S1A). Various crystal forms of full-length Sp-Cdc123 were obtained (Table S1). The 3D structure was solved using anomalous scattering data from crystals of selenomethionylated Cdc123, combined with non-crystallographic symmetry and multi-crystal averaging. The initial density map allowed us to trace most of the Cα backbone and identify non-crystallographic symmetry operators. This permitted partial refinement of a first 3D model of Sp-Cdc123 at 3.24 Å resolution. This model contained residues 2–271 with the exception of residues 51–71. The C-terminal part of the protein (272–319) was not visible in the electron density. We suspected that mobility of this region within the crystals might have hampered the diffraction quality. Therefore, a C-terminal truncated form of Sp-Cdc123 (1–274, hereafter named Sp-Cdc123Δc) was engineered. High-resolution diffracting crystals could be obtained using Sp-Cdc123Δc (Table 1). The structure was solved by molecular replacement using the 3.24-Å resolution model and refined to 2.06 Å resolution. Final statistics are given in Table 1. The final model contains two monomers of Sp-Cdc123Δc in the asymmetric unit. As in the case of the model obtained with the full-length protein, residues 51–71 were not defined in the electron density for both monomers, and loop 148–152 was difficult to model. Notably, the C-terminally truncated protein and the full-length protein were arranged as a tetramer within the crystals. Nevertheless, Sp-Cdc123 behaved as a monomer in solution, as shown by molecular sieving and conventional size-exclusion chromatography coupled to multi-angle static light scattering (SEC-MALS; see Experimental Procedures).

The structure of Sp-Cdc123Δc monomer can be divided into two α-β domains. The N-terminal domain contains residues 2–170 (domain 1) and the central domain contains residues 171–274 (domain 2, Figure 1). A comparison of the Sp-Cdc123 structure with other known structures was performed using the Dali server (Holm and Sander, 1995). All high-scoring entries in the PDB belonged to the ATP-grasp family. Representative top scoring matches are shown Figure S2B. All homologous structures shown in Figure S2B can be aligned to Cdc123 with *Z* scores ranging from 8.3 to 11.2 and root-mean-square deviation in the 3-Å range for 156–179 aligned residues. ATP-grasp enzymes catalyze similar reactions, involving an ATP-dependent ligation of a carboxyl group carbon with an amino or imino group nitrogen. Catalysis proceeds, in each case, through the formation of an acylphosphate intermediate (Artymiuk et al., 1996; Fan et al., 1995; Galperin and Koonin, 1997). This homology was unanticipated according to the low sequence similarities of Cdc123 with proteins of the ATP-grasp family (in the 10% range, Figure S2) and had previously not been detected using standard BLAST procedures. The classical ATP-grasp fold is formed of three domains usually named N, central, and C domains (or A, B, and C; Fawaz et al., 2011). The N domains are not structurally conserved between the various ATP-grasp enzymes. Comparison of ATP-grasp enzymes with Cdc123 (Figures 2 and S2) shows, however, that the structural homology is restricted to the central and C domains (equivalent to domains 1 and 2 in Cdc123, respectively; Figure 2C). Indeed, the N-terminal domain of ATP-grasp enzymes (colored gray in Figure S2B) is not observed in Cdc123 proteins. Domain 1 of Cdc123 contains a three-stranded β sheet, whereas the corresponding β sheet in ATP-grasp enzymes contains a fourth strand (Figure 2B). Residues forming this additional strand are inserted between β2 and β3 counterparts of Cdc123 domain 1 (Figure S2A). Domain 2 of Cdc123 contains a four-stranded antiparallel β sheet with a topology similar to that observed in the C-terminal domain of ATP-grasp enzymes (Figure S2). A fifth β strand is observed at the C-terminal part of Cdc123Δc. Finally, within domains 1 and 2, regions specific to Cdc123 are inserted or divergent (colored green in Figures 2 and S2). Among these are regions involved in ATP binding in grasp enzymes (colored orange in Figures 2 and S2; Fan et al., 1995).

Despite these differences, the obvious resemblance of Cdc123 with ATP-grasp enzymes suggested that Cdc123 had the ability to bind ATP.

Cdc123 Binds ATP

As an attempt to demonstrate ATP binding by Sp-Cdc123, a titration of the protein with ATP was followed using isothermal titration calorimetry (ITC) (see Experimental Procedures). A dissociation constant of 67 ± 13 μM could be deduced from the titration curve (Figure S3). This K_d value is in the same range as that measured for a typical ATP-grasp enzyme, the *S. aureus* D-alanine:D-alanine ligase (60 μM; Liu et al., 2006). This result shows that Sp-Cdc123 indeed binds ATP with significant affinity.

To obtain further insight into ATP binding, crystallization trials with Sp-Cdc123Δc were performed in the presence of ATP-Mg^{2+}, AMP-PNP-Mg^{2+}, and ADP-Mg^{2+}. Crystals isomorphic to crystals with unliganded Sp-Cdc123Δc were obtained and datasets collected. However, a bound nucleotide was only observed when crystals were prepared in the presence of adenylyl imidodiphosphate (AMP-PNP). In this case, there was no density for

Table 1. Data Collection and Refinement Statistics for Sp-Cdc123 Structure Determination

	Sp-Cdc123Δc	Sp-Cdc123Δc +ADP	Sp-Cdc123:Sc-γDIII +ATP-Mg^{2+}	Sp-Cdc123:Sc-γDIII
Data Collection				
Crystallization Conditions	4% tacsimate pH 5.0 12% PEG3350	4% tacsimate pH 5.0 12% PEG3350	0.2 M $LiSO_4$ 0.1 M Tris pH 8.0 25% PEG3350	0.2 M $LiSO_4$ 0.1 M Tris pH 8.0 25% PEG3350
Space group	C2	C2	$C222_1$	$C222_1$
Cell dimensions				
a, *b*, *c* (Å)	85.6, 91.7, 86.2	86.5, 91.4, 86.0	74.3, 116.6, 132.6	75.0, 117.4, 132.4
α, β, γ (°)	90, 93.5, 90	90, 91.4, 90	90, 90, 90	90, 90, 90
Resolution (Å)	45.8–2.06	43.2–1.85	45.0–2.9	45.7–3.0
R_{sym} (%)	5.0 (90.8)[a]	3.3 (47.4)	7.4 (87.5)	10.2 (117.3)
$I/\sigma I$	15.7 (1.3)	19.0 (2.7)	15.8 (2.2)	13.4 (2.0)
CC1/2 (%)	99.9 (77.5)	99.9 (78.6)	99.9 (80.4)	99.9 (87.4)
Completeness (%)	99.0 (94.3)	98.1 (96.4)	99.7 (99.3)	99.6 (97.8)
Redundancy	5.5 (5.1)	3.0 (2.9)	5.8 (5.9)	7.3 (7.0)
Refinement				
Resolution (Å)	45.8–2.06	43.2–1.85	45.0–2.9	45.7–3.0
No. of reflections	41,180	56,270	13,237	12,020
R_{work}/R_{free}	0.193/0.230	0.183/0.221	0.195/0.262	0.218/0.257
No. of atoms/B factors ($Å^2$)				
Protein	Mono1Cdc123 2075/57.9 Mono2Cdc123 2060/66.4	Mono1Cdc123 2096/35.5 Mono2Cdc123 2048/44.0	Cdc123 2288/101.7 γD3 805/100.0	Cdc123 2234/110.3 γD3 798/100.3
Water	198/62.5	331/44.3	5/72.8	
Ligand		ADP-Mono1 27/38.4	ATP 31/82.1 Mg 1/72.6	
Root-mean-square deviations				
Bond lengths (Å)	0.008	0.008	0.009	0.008
Bond angles (°)	1.09	1.10	1.18	1.05

A single crystal was used for data collection.
[a]Values in parentheses are for the highest-resolution shell.

the γ-phosphate group in the maps; therefore, the density was assigned to an ADP molecule. Instability of AMP-PNP in acidic conditions has been reported (Sigma-Aldrich product information sheet) and could explain the presence of ADP instead of AMP-PNP. Only one ADP molecule bound to monomer A was clearly identified (Table 1; Figure 3). No magnesium ion bound to ADP was observed. In monomer B, residual electron density within the pocket was attributed to water molecules. Their positions may reflect low occupancy of ADP. Packing constraints may possibly have hampered tight binding of ADP to the second monomer.

In monomer A, ADP is bound in a position corresponding to the ATP binding pocket previously identified in ATP-grasp enzymes, at the interface between domain 1 and domain 2 (Figures 1 and 2). One side of the ADP molecule is held by residues located in domain 2 of Cdc123, belonging to motifs conserved in all ATP-grasp enzymes (yellow residues in β4–β7, Figure 3A). At the opposite side, some residues belonging to domain 1 participate in the binding of ADP (residues 164–167, blue residues in Figure 3A). Additional contacts involve residues located in non-conserved regions (residues 99, 101, 103, colored green in Figure 3A). Interestingly, the two regions corresponding to the loops involved in ATP binding in ATP-grasp enzymes, named "small loop" and "large loop" (Figures 2B and S2, residues 176–180 and 233–261 in 1E4E), are highly divergent in Cdc123. These two regions of ATP-grasp enzymes form a lid in the presence of ATP, interacting together above the ATP binding cavity (Figures 2B and S2; Fan et al., 1995; Hara et al., 1996; Roper et al., 2000; Zhao et al., 2013). In place of the small loop segment, region 98–110 contains stretches of residues highly conserved in Cdc123 proteins (Figure S1). Finally, comparison of the structure of unliganded Cdc123 with that of ADP-bound Cdc123 only showed adjustments of side chains involved in the binding of ADP.

Overall, analysis of the ADP binding site in Cdc123 shows that nucleotide binding involves regions and residues of the protein that are conserved in ATP-grasp enzymes (Figure S2). This observation makes a strong case for a common ancestry of Cdc123 and ATP-grasp enzymes. However, significant differences are observed within their respective ATP binding sites.

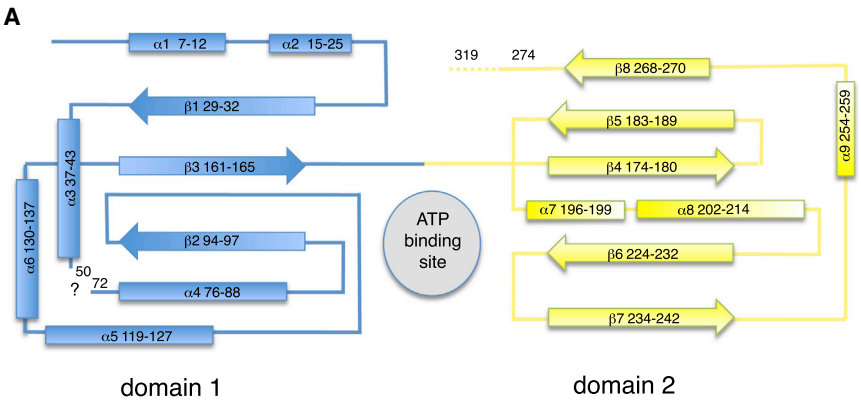

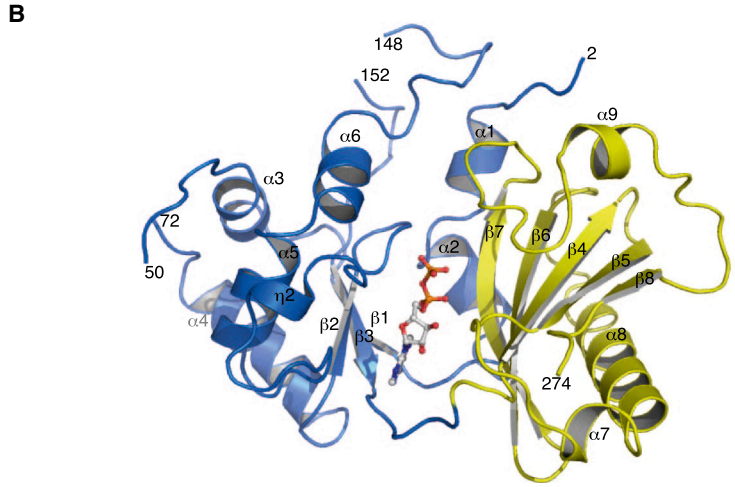

Figure 1. Structure of Sp-Cdc123

(A) Schematic representation of the topology of Sp-Cdc123Δc. The β strands are represented as arrows and the helices as rods. Secondary structure elements were assigned with PROCHECK (Laskowski et al., 1993). Domain 1 is colored blue (residues 1–170) and domain 2 is colored yellow (residues 171–274).

(B) Cartoon representation of Sp-Cdc123Δc. Same color code as in (A). ADP is shown as sticks. Secondary structure elements are labeled. All structural views are drawn with PyMol (Schrodinger, 2010).

See also Figure S1.

Such divergences are likely to be linked to the biological function of Cdc123. Overall, Cdc123 may be considered as an atypical member of the ATP-grasp family.

Notably, a second cavity faces the nucleotide binding pocket in Cdc123 (Figure 3). This cavity is walled by residues V10, C13, and Q14 from α1 on one side and by residues H134, D135, and F140 from α6 on the other side. In addition, the side chains of R246 and W99 are positioned at the top and bottom of the cavity, respectively. In the ADP-bound structure, the cavity is filled up by electron density attributed to five water molecules. According to the location of the second binding pocket and the homology with the ATP-grasp enzymes, it is conceivable that this pocket corresponds to a binding site for a second ligand of Cdc123, substrate of a reaction involving an ATP-dependent ligation step as observed in ATP-grasp enzymes. The existence of such an unidentified second ligand remains, however, hypothetical at this stage.

Binding of Cdc123 to eIF2γ

In vivo assembly of the eIF2 complex was shown to depend on Cdc123. Sc-Cdc123 activity involved an interaction with the unassembled eIF2γ subunit (Perzlmaier et al., 2013). eIF2γ is made of three domains: the GTP binding domain, γDI, and the two β barrels γDII and γDIII (Schmitt et al., 2010). Within eIF2γ, domain III was shown to be sufficient for binding to Cdc123 (Perzlmaier et al., 2013).

According to these results, we demonstrated an in vitro interaction of Sc-Cdc123 to the Sc-eIF2γDIII domain (domain III of eIF2γ from *S. cerevisiae*) using molecular sieving experiments (Figure S3; Experimental Procedures). Interestingly, the behavior of Sc-Cdc123 on the molecular sieve column suggested that the protein was dimeric in its unliganded form and became monomeric upon binding to eIF2γDIII (Figure S3). The K_d value for the binding of Sc-eIF2γDIII to Sc-Cdc123 was 2.5 ± 0.5 μM, as measured using ITC (Figure S3). This value was measured in the absence of ATP. Hence, binding of Sc-eIF2γDIII to Sc-Cdc123 did not strictly require the presence of ATP-Mg^{2+}. Despite several attempts, no crystal could be obtained using the purified complex. Therefore, we decided to design a chimeric complex made of Sp-Cdc123 bound to Sc-eIF2γDIII. Formation of a stable complex was indeed observed by a pull-down experiment showing that an N-terminally His-tagged version of Sp-Cdc123 can trap Sc-eIF2γDIII on a cobalt affinity resin. Upon elution with imidazole, a peak corresponding to a heterodimer of Sp-Cdc123 bound to Sc-eIF2γDIII was observed (see Experimental Procedures). An additional step using molecular sieving allowed us to polish the purification (Figure S3). Notably, the binding of Sc-eIF2γDIII to Sp-Cdc123 did not produce sufficient heat changes to allow accurate determination of a K_d value using ITC. One possible explanation is that, in the case of the complex formed with the *S. cerevisiae* proteins, binding of Sc-Cdc123 to Sc-eIF2γDIII is accompanied by a change of the oligomeric state of Sc-Cdc123 from homodimer to monomer. Sp-Cdc123 behaves as a monomer, and binding to Sc-γDIII does not change its oligomeric state, possibly explaining why observed heat changes are weaker.

Suitable crystals were obtained using the purified complex Sp-Cdc123:Sc-eIF2γDIII at 24°C in the presence or absence of ATP-Mg^{2+}. The structure was solved by molecular replacement using the structure of Sp-Cdc123Δc determined in this study and the structure of aIF2γDIII from *Sulfolobus solfataricus*

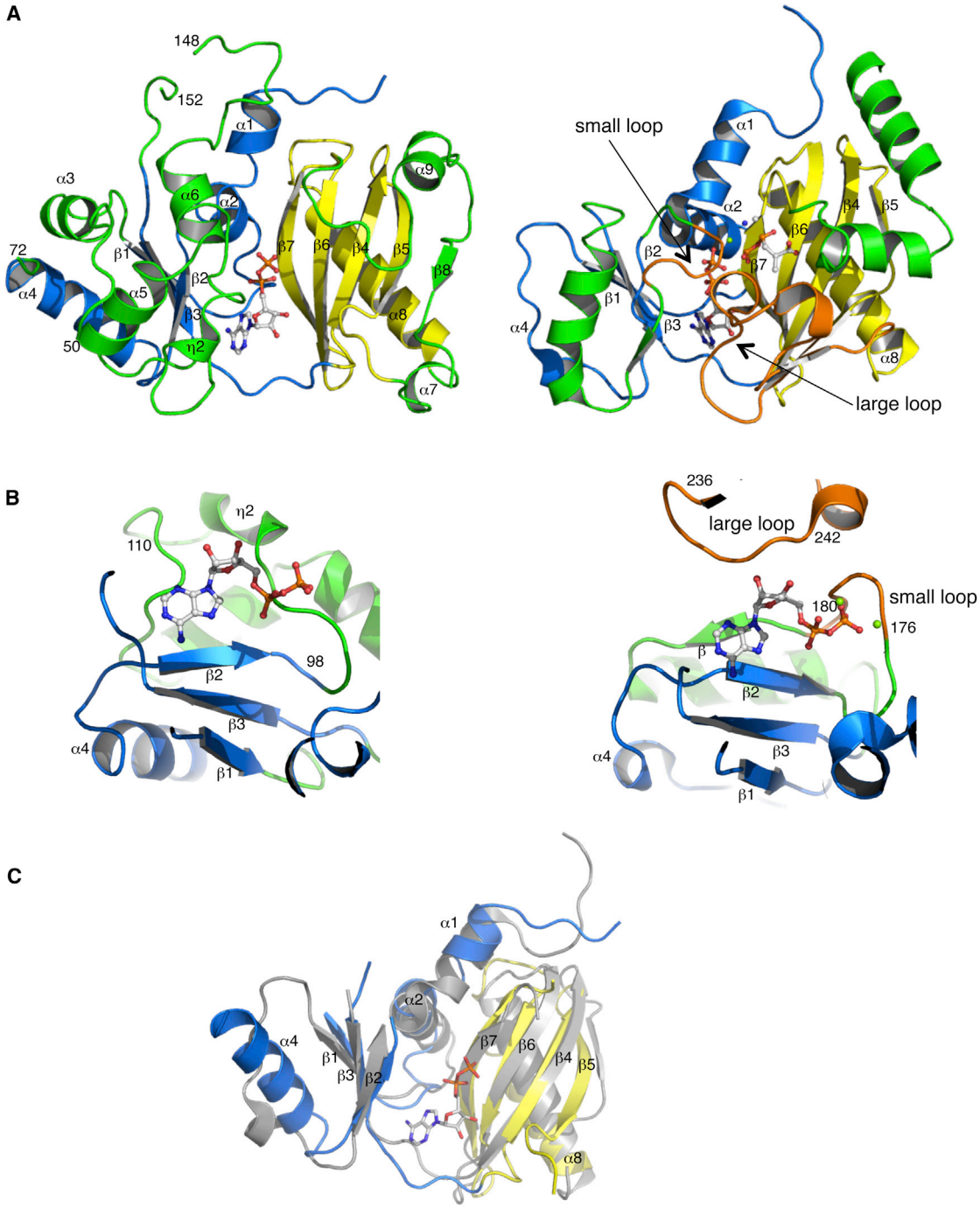

Figure 2. Comparison of sp-Cdc123 with D-Alanyl-D-Lactate Ligase from ATP-Grasp Superfamily

(A) Left: Cartoon representation of Sp-Cdc123Δc. Domain 1 is colored blue and domain 2 is colored yellow except for regions specific to Cdc123 proteins, which are green. ATP is shown in sticks. Right: Cartoon representation of (VanA) from *Enterococcus faecium* (PDB: 1E4E; Roper et al., 2000). For the sake of clarity, the N-terminal domain is not represented. Parts of the central domain of 1E4E similar to Cdc123 are colored blue, and parts of the C domain of 1E4E similar to Cdc123 are colored yellow. Divergent regions compared with Cdc123 are shown in green. The small and large loops overhanging ATP are shown in orange. ATP and a phosphorylated inhibitor bound to VanA are shown as sticks and spheres. The magnesium ion is shown as a green sphere.

(B) Left: Close-up view of the domain 1 of Sp-Cdc123 showing the three-stranded β sheet. Right: Close-up view of the central domain of 1E4E showing the four-stranded β sheet and the two loops surrounding ATP. The color code is the same as in (A). This view highlights the differences within the ATP binding site between Cdc123 and the representative from the ATP-grasp family.

See also Figure S2.

(C) Superimposition of the ATP-grasp core domain of Cdc123 (in blue and yellow, as in A) onto the corresponding one in 1E4E (in gray). For the sake of clarity, divergent regions have been omitted.

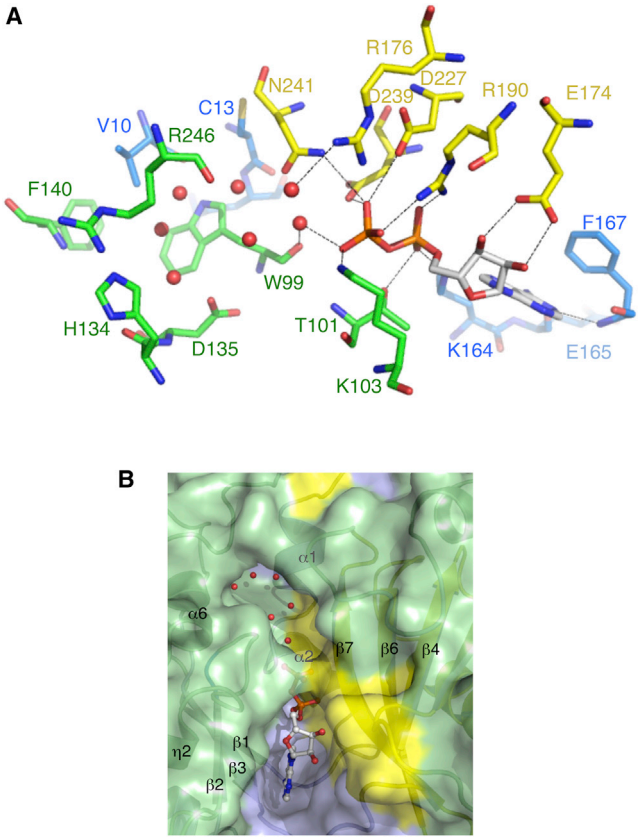

Figure 3. Binding of ADP to Sp-Cdc123Δc

(A) The residues involved in ADP binding and the corresponding electrostatic bonds are shown. Color code is the same as in Figure 2A. Water molecules are shown as red spheres.

(B) Molecular surface representation of Sp-Cdc123Δc. Color code is the same as in Figure 2A. The view highlights the second cavity facing the ATP binding pocket.

See also Figure S3.

(PDB: 2AHO; Yatime et al., 2006) as search models. The structures were refined to 2.9 and 3.0 Å resolution in the presence or absence of ATP-Mg^{2+}, respectively (Table 1).

Within the complex, the structure of the γDIII domain was defined from residues 423 to 524 with only the three C-terminal residues not visible in the electron density. In Sp-Cdc123, all residues corresponding to the two core domains (from 2 to 274) were visible with the exception of two loops (residues 53–68 and 149–152). Residues 275–296 were not visible. However, additional electron density disconnected from the main structure was attributed to a long helix of the C-terminal domain of Sp-Cdc123 (α10, residues 297–315). Superimposition of the structure of the complex obtained in the presence of ATP on that obtained without ATP showed only adjustments of side chains involved in the binding of ATP.

Overall Structure of Sp-Cdc123:Sc-eIF2γDIII

Sc-eIF2γDIII forms a β barrel highly homologous to the corresponding domain in archaeal aIF2 (Figure S4). Two differences are notable: in the eukaryotic domain, (1) the loop between β16 and β17 is longer and (2) β21 is extended by four residues in such a way that its interaction with strand β16 is reinforced.

In the structure of the complex, the γDIII domain is bound to one side of Cdc123 domain 1. Neither Cdc123 domain 2 nor the C-terminal helix α10 contacts γDIII (Figure 4A). γDIII and Cdc123 closely interact with an interaction surface of 1,307 $Å^2$. Interestingly, the binding site of γDIII to Cdc123 overlaps the dimerization site of Cdc123 observed in all crystal forms. To address the possibility that the observed position of γDIII to Cdc123 may have resulted from crystallization artifacts, a solution study was carried out using small-angle X-ray scattering (SAXS). The goal was to compare the theoretical X-ray scattering curve deduced from the crystallographic structure with the scattering curve experimentally observed in solution. As shown in Figure 4B, the SAXS experimental curve obtained with the purified Sp-Cdc123:Sc-eIF2γDIII fits very nicely the curve calculated from the crystal structure coordinates. This strongly argues in favor of the biological significance of our crystalline model.

Detailed interactions of Sp-Cdc123 with Sc-eIF2γDIII are shown in Figures 4C and 4D. Sc-eIF2γDIII is mainly bound through its concave side formed by strands β17-β18-β19-β20-β21 of the barrel and by the β20-β21 loop (Figure 4D). On the side of Cdc123, the main regions of contacts correspond to α3 and the following loop (residues 44, 46–50), helix η2 (residues 107–110), α5, and α6 (Figure 4C). Notably, the Cdc123 regions involved in the binding of Sc-eIF2γDIII correspond to regions specific to Cdc123 proteins, not found in ATP-grasp enzymes (Figures 2 and S2, green regions). Figure S1, Figure S4, and Table 2 show residues involved in the heterodimer interface between Cdc123 and γDIII. Superimposition of bound Cdc123 on unbound Cdc123 showed that binding to γDIII involved adjustment of the interface regions. In particular, α3 and the following loop are displaced and the conformation of the region around helix η2 (residues 107–110) is adjusted. This part of Cdc123 is connected to the ATP binding pocket (Figures 4C and 4D). Nevertheless, the K_d value of ATP measured by ITC for Sp-Cdc123:Sc-eIF2γDIII (57 ± 7 μM) was not significantly changed compared with that measured for isolated Sp-Cdc123 (67 ± 13 μM).

Previous results had suggested that within domain III, the C-terminal tail, specific to eukaryotic eIF2γ, was required for the interaction with Cdc123. Indeed, removal of 13 amino acids at the C-terminal extremity of eIF2γ (residues 515–527) was sufficient to render the protein non-functional in the binding to Cdc123 or to eIF2α and eIF2β subunits (Perzlmaier et al., 2013). On the contrary, the removal of four amino acids from the C terminus was tolerated, since binding to Cdc123 and assembly with α and γ subunits still occurred (Perzlmaier et al., 2013). No direct interaction is observed between the C-terminal part of γDIII and Cdc123 in the structure of the complex. However, the structure shows that the last β strand of γDIII (β21) is extended to residue 522. Therefore, it is likely that a deletion of residues belonging to β21 led to destabilization of the structure of the β barrel and thereby impaired binding to Cdc123. According to these observations, the absence of C-terminal extension in archaeal aIF2γDIII cannot be straightforwardly related to the absence of Cdc123 from archaea.

To further characterize the complex between Cdc123 and eIF2γDIII, mutations within γDIII were introduced. Three single

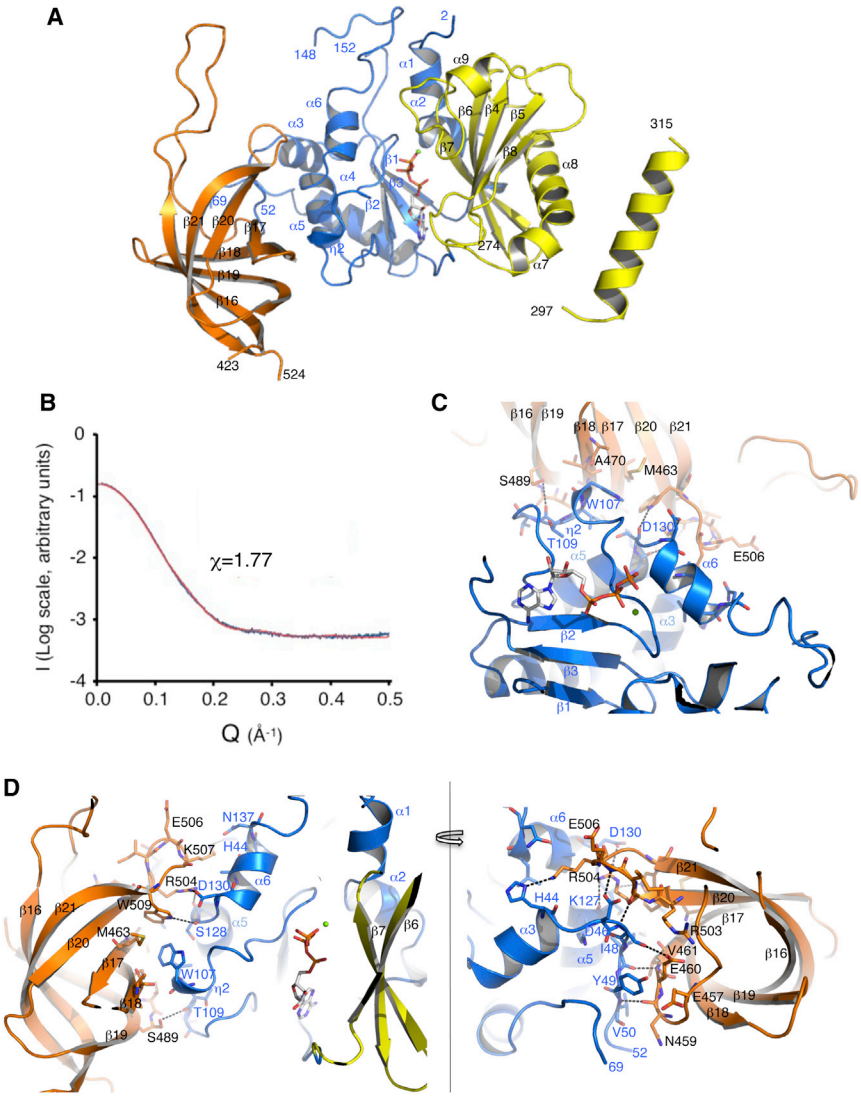

Figure 4. Structure of Sp-Cdc123:Sc-eIF2γ DIII Complex

(A) Overall structure of Sp-Cdc123:Sc-eIF2γDIII complex. Sp-Cdc123 is colored as in Figure 1B. ATP is shown as sticks and Mg^{2+} as a green sphere. Sc-γDIII is colored orange.

(B) Solution studies using SAXS. The experimental SAXS curve (blue) is compared with the theoretical diffusion curve deduced from the crystalline structure of Sp-Cdc123:Sc-γDIII complex (red).

(C) Close-up view of Sp-Cdc123:Sc-γDIII showing the proximity of the ATP binding pocket with the interface between the two proteins.

(D) Detailed interactions between Sp-Cdc123 and Sc-γDIII. The residues involved in the stabilization of the interface between the two proteins and the corresponding electrostatic interactions are shown (see also Table 2). The right view is rotated by 180° compared with the left view.

See also Figure S4.

mutants were produced, E460A, R504A, and W509A. The effect of the mutations on association with Sp-Cdc123 was evaluated using pull-down assays (Figure S4). As predicted from the 3D structure, modification of R504 and W509 into alanine resulted in a lower amount of Sp-Cdc123:Sc-eIF2γDIII complex retained on the affinity column, compared with that obtained with wild-type Sc-eIF2γDIII (Figure S4). In the case of E460A mutant, a lower level of protein expression did not allow us to reach a firm conclusion.

ATP Binding Residues of Cdc123 Are Crucial for eIF2 Assembly

Crystals of Sp-Cdc123:Sc-eIF2γDIII complex could be obtained in the presence of ATP-Mg^{2+} (Table 1). As shown in Figures 5 and S5A, ATP-Mg^{2+} is observed, firmly bound to Cdc123 in the presence of one Mg^{2+} ion. The octahedral coordination of the tightly bound magnesium ion is visible. In the equatorial plane, four bonds involve D239 and N241 side chains and two oxygens from the β and γ phosphate groups. Two water molecules are in apical positions. One of them is stabilized by D227, whereas the second water appears less stable. Superimposition of Sp-Cdc123:Sc-eIF2γ DIII:ATP on Cdc123Δc:ADP shows that the two structures are nearly identical in the area of the nucleotide, with only adjustments of side-chain residues involved in the binding of Mg^{2+} and the γ-phosphate group (Figure S5B).

Interestingly, in line with the γ-phosphate of ATP is a water molecule located at 3.3 Å from the oxygens, at the entrance of the second cavity. This water molecule, stabilized by interactions with the main-chain NH group of D248 and the side-chain NH_2 group of R176, would be correctly positioned to participate in a possible ATP hydrolysis reaction (Figures 5A and S5B). At present, however, such an activity has not been firmly established.

To obtain further insight into the role of ATP in eIF2 assembly, mutants of Sc-Cdc123 were designed and their behaviors studied in vivo.

We targeted residues involved in the coordination of the ATP-bound Mg^{2+} ion. Indeed, these residues (D227, D239, N241 in Sp-Cdc123) are highly conserved in Cdc123 sequences and ATP-grasp enzymes (Figures S1 and S2). Moreover, various studies of ATP-grasp enzymes have shown that these residues are essential for the enzymatic activity, and have suggested that Mg^{2+} has a catalytic role by maintaining ATP in a correct conformation for catalysis (Miller et al., 2005; Sloane et al., 2001). Therefore, we mutated the "DIN" sequence of Sc-Cdc123 (DIN; 266–268 in Sc-Cdc123 corresponding to 239–241 in Sp-Cdc123, Figure S1) into three alanines. To test the effect of the DIN mutation in vivo, we used a diploid yeast cells heterozygote for a *CDC123* gene deletion, expressing either the wild-type *CDC123* or the DIN mutant (Figure 5B, right panel). No complementation of a deletion of the *CDC123* gene was observed in the presence of the Sc-Cdc123 DIN. Moreover, the DIN mutant also failed to support

Table 2. Summary of Interactions Involved in the Binding of γDIII Domain to Cdc123

Sp-Cdc123	Sc-γDIII	Distances (Å)
Electrostatic Bonds		
H44 Nδ1	K507 Nε	3.1
D46 Oδ2	E506 N (mc)	3.0
S47 Oγ	E460 Oε2	3.2
I48 O (mc)	V461 N (mc)	2.7
V50 N (mc)	N459 O (mc)	3.0
S47 N (mc)	R504 O (mc)	2.8
K127 O	R504 Nh1	3.3
D130 Oδ1	R504 Nh2	2.7
S128 O (mc)	W509 Nε	3.3
Non-bonded Contacts		
Y49	E457	
W107	M463-A470-T471-G472	
I108	T488-S489	
T109	T488-S489	
T110	T488-S489	
A133	K507	
L136	K507	
N137	K507	
L43	K507	
S47	R503	
D46	I505	

assembly of Sc-eIF2γ with eIF2α (Figure 5B, left panel). This observation was made in an *S. cerevisiae* strain deleted for *CDC123* and kept alive by high-level expression of eIF2γ and eIF2α. Relative to a strain that carries the *CDC123* gene, there was much less eIF2γ-eIF2α association in the *cdc123* deletion mutant. Expression of the wild-type version of Cdc123 restored normal eIF2γ-eIF2α association. Expression of the Sc-Cdc123 DIN mutant, however, failed to increase the association of eIF2γ with eIF2α (Figure 5B, left panel). Thus, ATP binding residues are essential for Cdc123 to support cell viability and eIF2γ-eIF2α assembly. Using co-IP experiments, we observed a defect of the DIN mutant in its interaction with full-length eIF2γ, whereas the amount of co-precipitated eIF2α was unaffected by the DIN mutation (Figure S6A). This indicates a link between ATP and the binding of full-length eIF2γ by Cdc123.

To substantiate these observations, we analyzed another mutant of the ATP binding site of Cdc123, Sc-CDC123-D252A (equivalent to *S. pombe* D227) mutant. This residue, as D266 and N268, participates in the binding of the magnesium ion through a water-mediated interaction (Table 3). In line with the DIN mutant, Sc-CDC123-D252A failed to complement a *CDC123* gene deletion and did not support assembly of eIF2γ with eIF2α (Figure 5B). Together, these data show that the DIN and D252A mutations disrupt both the biological and biochemical function of Cdc123. Hence, these results strongly argue in favor of a requirement on ATP binding for the vital cellular function of Cdc123 and its role in promoting eIF2αγ assembly.

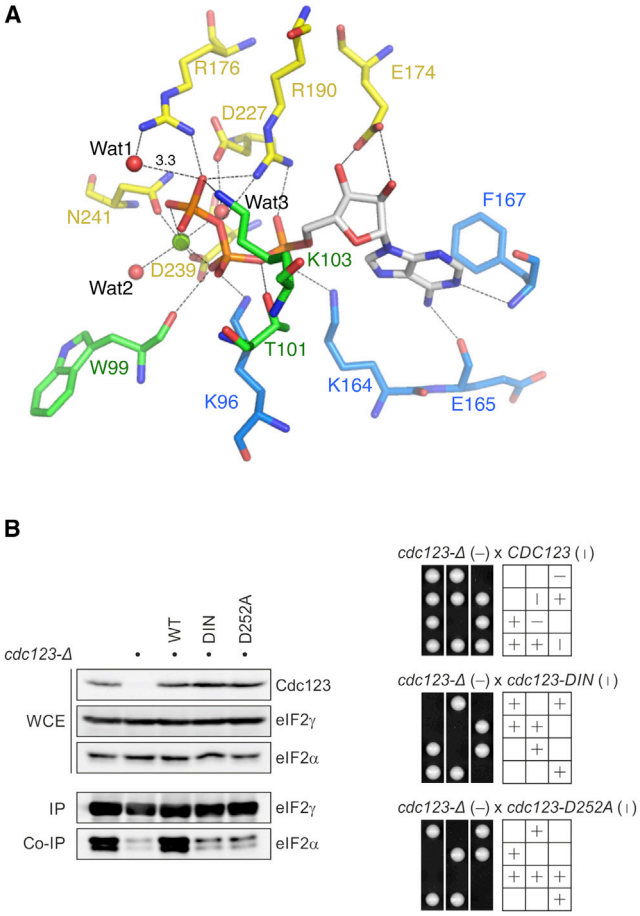

Figure 5. Binding of ATP-Mg^{2+} to Sp-Cdc123:Sc-γDIII Complex

(A) The residues involved in ATP binding and the corresponding electrostatic interactions are shown. Color code is the same as in Figure 3A. Water molecules are shown as red spheres and the magnesium ion as a green sphere.

(B) Right: Failure of Cdc123-DIN (DIN266-268AAA) and Cdc123 D252A to support cell viability. Diploid yeast cells heterozygote for a *CDC123* gene deletion and expressing either a wild-type copy of *CDC123* (upper panel; W14145), DIN (DIN266-268AAA; middle panel; W13936), or D252A (lower panel; W13935) mutant versions of *CDC123* were sporulated and subjected to tetrad dissection. Left: Failure of Cdc123-DIN (DIN266-268AAA) and Cdc123 D252A to support interaction of eIF2γ with eIF2α. Yeast strains overexpressed flag3-eIF2γ/Gcd11 and eIF2α/Sui2, and either carried the endogenous wild-type copy of *CDC123* (W7743; lane 1) or were deleted for *CDC123* (*cdc123-Δ*; lanes 2–5; W7745 lane 2) and expressed a wild-type copy (W13930; lane 3), the DIN (W13931; lane 4), or the D252A mutant version of *CDC123* (W14238; lane 5). Proteins were detected by western analysis in whole-cell lysates (WCE) and anti-flag immunoprecipitates (IP).

See also Figure S5.

Model for the Catalytic Complex

To promote our understanding of the mechanism used by Cdc123 for eIF2 assembly, we performed a docking model for the binding of eIF2γ onto Cdc123. According to structural alignments and biochemical data, the 3D structure of the eukaryotic γ subunit is supposed to be very close to that of its archaeal counterpart (Schmitt et al., 2012). Therefore, to make the docking model, the Sc-eIF2γDIII domain from the Sp-Cdc123:γDIII structure was superimposed on the corresponding domain in

Table 3. Summary of Interactions Involved in the Binding of ATP to Sp-Cdc123:Sc-γDIII

Sp-Cdc 123	ATP Binding Sp-Cdc123:Sc-γDIII	Distances (Å)
Electrostatic Bonds		
K96 Nε	O1α	2.9
	O2β	3.3
T101 Oγ1	O3α	3.0
	O1β	2.8
K164 Nε	O1α	2.8
	N7 adenine	2.9
E165 O (mc)	N6 adenine	3.0
F167 N (mc)	N1 adenine	3.2
E174 Oε1	O2′ ribose	3.3
Oε2	O3′ ribose	2.9
R176	O3γ	3.0
R190 Nh1	O2α	2.8
Nh2	O3γ	2.9
D227 Oδ2	Wat3	2.7
D239 Oδ2	Mg^{2+}	2.1
	O2β	2.9
N241 Oδ1	Mg^{2+}	2.2
Wat2	Mg^{2+}	2.7
Wat3	Mg^{2+}	2.5
Non-bonded Contacts		
K103	O1γ	
	O1β	
S100	O1γ	
	O1β	
I238	O1β	
	O2β	
L114	O4′ ribose	
W166	N6 adenine	
	N1 adenine	
	C2 adenine	
V94	N6 adenine	
M169	C8 adenine	
	N7 adenine	
	C5 adenine	

aIF2γ structure (PDB: 4RD4; Dubiez et al., 2015). In this model, shown in Figures 6A and 6B, the complete eIF2γ subunit is nicely anchored to Cdc123, without intertwining. Interestingly, the docking model revealed another potential contact between eIF2γ and Cdc123. This contact would involve the long L1 loop of aIF2γ-DII domain and the loop linking β5 to α7 (residues 192–196) of Sp-Cdc123. Strikingly, L1 loop of e/aIF2γ-DII domain is known to mediate interaction between e/aIF2γ and e/aIF2α subunits (Naveau et al., 2013; Roll-Mecak et al., 2004; Schmitt et al., 2002; Yatime et al., 2006).

Importantly, the position of eIF2γ on Cdc123 is compatible with simultaneous binding to eIF2α. Indeed, the docking model can be completed by positioning the aIF2α subunit, thanks to the knowledge of the aIF2αγ structure (PDB: 2AHO; Yatime et al., 2006). As shown in Figure 6C, the model suggests an interaction of Cdc123 with the interface between α and γ subunits. Hence, the docking model opens the possibility that Cdc123 acts through transient interaction with the L1 loop of γDII and domain 3 of eIF2α subunit. This interaction would be necessary for the assembly of eIF2γ and eIF2α.

To test the docking model, we generated a mutant version of eIF2γ lacking part of the L1 loop and analyzed its interaction with Sc-Cdc123 and the α and β subunits in a yeast two-hybrid (Y2H) assay. The L1 loop mutation had little or no effect on the interaction of eIF2γ with eIF2β, but disrupted the interaction of eIF2γ with eIF2α and reduced the interaction of eIF2γ with Cdc123 (Figure S6B). The Y2H data, therefore, confirm the L1 loop region as an α-γ binding site in eukaryotic eIF2 orthologs, and supports the notion of a physical contact between the L1 loop of eIF2γ and Cdc123, as predicted by the docking model.

To further analyze the docking model, we considered an interaction of Sc-Cdc123 with eIF2α. To this end, we overexpressed a flag3-tagged version of Sc-Cdc123 in a yeast strain whose endogenous eIF2α-encoding gene was fused to a myc13-tag. Indeed, eIF2α-myc13 was detected in anti-flag immunoprecipitates of Cdc123. This signal was specific because it was absent from precipitates of a control strain, which lacked Cdc123-flag3 but expressed eIF2α-myc13 (Figure S6A). This experiment demonstrates a contact between Cdc123 and eIF2α or eIF2αγ. Compared with the relative amount of eIF2γ co-precipitated with Cdc123-flag3 from cell extracts, much lower levels of eIF2α-myc13 were recovered. The Cdc123-eIF2α or -eIF2αγ contact might therefore be transient.

DISCUSSION

This study revealed the 3D structure of the cell proliferation protein Cdc123. This protein resembles enzymes belonging to the ATP-grasp superfamily. As suggested by this resemblance, ATP binding to Cdc123 could indeed be demonstrated using biochemical tools and 3D structure determination. ATP is bound by residues common to Cdc123 and ATP-grasp enzymes but also by residues specific to Cdc123. Moreover, ATP-grasp enzymes possess an N-terminal domain, which constitutes part of their catalytic center. This domain is absent in Cdc123. Overall, Cdc123 protein appears as a member of the ATP-grasp family with unique features.

As in ATP-grasp enzymes, crucial residues are involved in the binding of the magnesium ion held on ATP. These residues (D252, D266, N268 in Sc-Cdc123 equivalent to D227, D239, N241 in Sp-Cdc123) were shown in this study to be essential for the cellular function of Cdc123. In the same vein, it should be remembered that a temperature-sensitive mutant of a rat fibroblast line, arrested in the G1 phase of the cell cycle at restrictive temperature, was mapped within Cdc123 (Ohno et al., 1984; Okuda and Kimura, 1996). The mutation identified corresponds to a change of A109 into valine (equivalent to T101 in Sp-Cdc123). T101 indeed participates in the binding of ATP (Table 3). Therefore, this temperature-sensitive mutant gives further credit to the idea that ATP is needed for the cellular function of Cdc123.

Previous studies had shown that Cdc123 was necessary for eIF2 assembly (Perzlmaier et al., 2013). In particular, interaction between unassembled eIF2γ and Cdc123 was shown, with DIII domain of eIF2γ being sufficient to trap Cdc123. Here, we

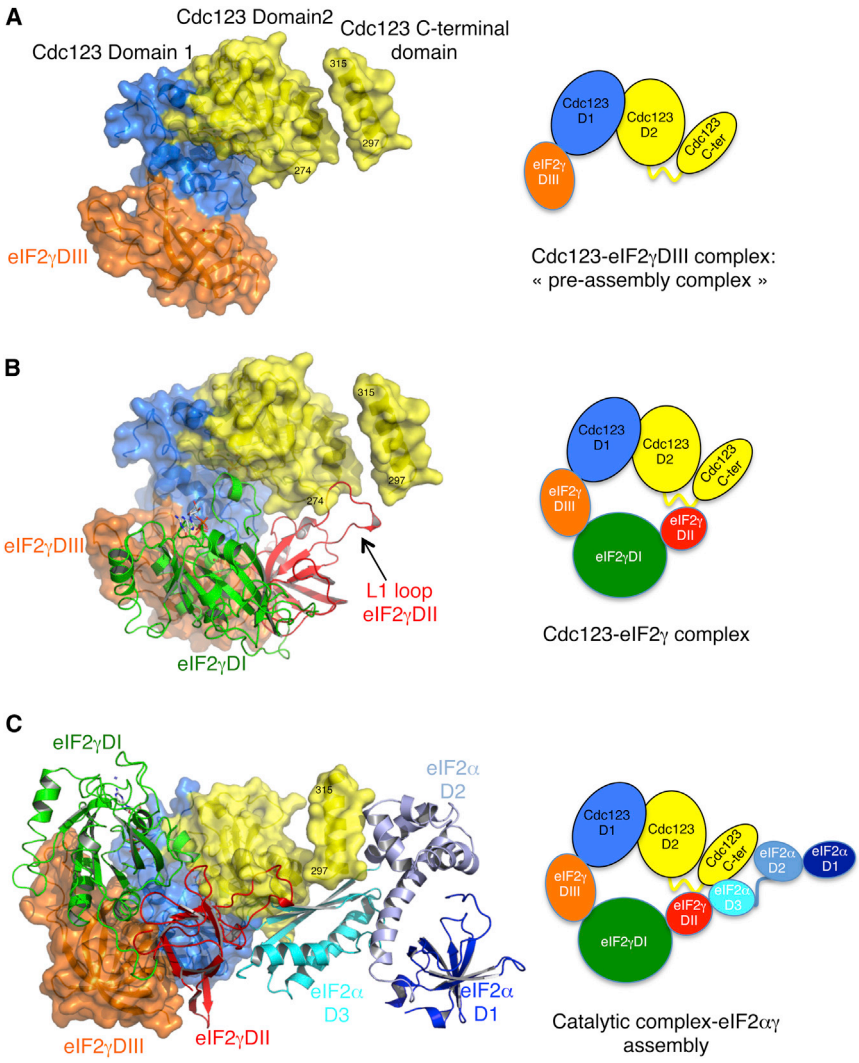

Figure 6. Model for the Binding of Cdc123 to eIF2αγ

(A) Molecular surface representation of Sc-Cdc123:Sc-eIF2γDIII complex. Color code is the same as that used in Figure 4.

(B) Docking of aIF2γ onto Sp-Cdc123. Sc-eIF2γ DIII domain from the Sp-Cdc123:γDIII structure was superimposed on the corresponding domain in aIF2γ structure (PDB: 4RD4; Dubiez et al., 2015). Sp-Cdc123:γDIII is colored as in (A). Domain I of aIF2γ is colored green, domain II of aIF2γ is colored red. An arrow indicates the long L1 loop responsible for the binding of aIF2γ to aIF2α (Yatime et al., 2006).

(C) Docking of aIF2αγ onto Sp-Cdc123. Sc-eIF2γDIII domain from the Sp-Cdc123:γDIII structure was superimposed on the corresponding domain in aIF2αγ structure (see text, PDB: 2AHO; Yatime et al., 2006). Color code is the same as in (B) for aIF2γ and Cdc123. aIF2α is colored as follows: domain 1, dark blue; domain 2, light blue; domain 3, cyan.

On the right of the structural views are schematics illustrating domain contacts within models of Cdc123:eIF2γ and Cdc123:eIF2αγ complexes. See also Figure S6.

determined the structure of Sp-Cdc123 bound to the γDIII domain of eIF2. The γDIII domain of eIF2 is bound to Cdc123 via interactions involving only Cdc123 domain 1. Domain 2 and the C-terminal domain do not contact γDIII. This observation is consistent with results obtained using a Y2H assay and IP experiments, showing that C-terminal sequences of Sc-Cdc123 are dispensable for γ binding (Figure S6C). On the contrary, this C-terminal region is essential for Cdc123 function because cells carrying Cdc123Δ291 are inviable (Figure S6C). Association of the eIF2 subunits was consistently compromised when a truncated version of Sc-Cdc123 (Sc-Cdc123Δ327) was used (Perzlmaier et al., 2013).

Accordingly, the docking model suggests that the C-terminal domain of Cdc123 is involved in the assembly process of eIF2γ to eIF2α. Therefore, eIF2γ would be bound to Cdc123 by an anchoring point located in domain 1 of the Cdc123, as observed in the present Cdc123-γDIII structure. From this viewpoint, the Cdc123-γDIII structure might represent a "pre-assembly complex" (Figure 6). A second contact point, possibly dependent on ATP binding and/or ATP hydrolysis, involving domain 2 and the C-terminal domain of Cdc123 would be necessary for the reshaping of the interaction surface between eIF2γ and eIF2α. Once assembled, the eIF2αγ complex becomes stably folded, allowing further spontaneous binding of the eIF2β subunit without the help of Cdc123 (Perzlmaier et al., 2013; Our unpublished data). After assembly, Cdc123 no longer interacts with eIF2 (Perzlmaier et al., 2013) even though the region of γDIII involved in Cdc123 interface remains accessible (Figure 6C). This suggests that the release of Cdc123 might result from unfavorable interactions between the second contact point (domain 2 and C-terminal domain of Cdc123) and the reshaped eIF2αγ association surface.

Notably, archaea do not display Cdc123 orthologs. Accordingly, assembly of aIF2 subunits occurs spontaneously in vitro (Pedulla et al., 2005; Stolboushkina et al., 2008; Yatime et al., 2004, 2006). However, Sequence alignments highlighting the specificities of eukaryotic and archaeal e/aIF2γ do not give any obvious clue to explain the different behaviors of eIF2 and aIF2 regarding the assembly of the heterotrimer (Yatime et al., 2007).

Affecting the binding of ATP to Cdc123 led to the loss of Cdc123 function. Thus, our structural and biochemical data link the function of Cdc123 in eIF2 assembly to the cell energetics. This reinforces the idea that Cdc123 is an important control point of the eukaryotic cell cycle. The question of whether Cdc123 uses ATP in a chaperone-like fashion to support eIF2αγ assembly without covalent modification, or whether Cdc123 uses ATP to introduce a post-translational modification in an effector site, remains open. The existence of a second binding pocket identified in the structure rather argues in favor of the

second possibility. However, our current attempts to demonstrate modification in purified eIF2γ subunit from cells expressing or not expressing Cdc123 have been fruitless. Therefore, further studies are clearly required to reveal how Cdc123 uses ATP to favor the assembly of eIF2.

EXPERIMENTAL PROCEDURES

Protein Expression and Purification

Sp-Cdc123

The gene coding for Sp-Cdc123 was amplified from a cDNA library (a generous gift from François Lacroute, INRA, Grignon, France) and cloned into pET3a and pET15b derivatives. The resulting plasmids, called pET3a-SpCdc123 and pET15b-SpCdc123, led to the expression of an untagged and an N-terminally tagged version of Sp-Cdc123, respectively. To express the protein, the desired plasmid was transformed into *E. coli* BL21 Rosetta pLacI-Rare (Merck, Novagen). One-liter cultures were grown in 2xTY medium containing 50 μg/ml ampicillin and 34 μg/ml chloramphenicol. Expression was induced by adding 1 mM isopropyl β-D-1-thiogalactopyranoside in an overnight 37°C culture. After induction, the cultures were continued for 5 hr at 18°C. For untagged Sp-Cdc123, cells corresponding to 1 l of culture were disrupted by sonication in 30 ml of buffer A (10 mM HEPES [pH 7.5], 200 mM NaCl, 3 mM 2-mercaptoethanol, 0.1 mM PMSF, 0.1 mM benzamidine). The crude extract was loaded onto a Q-Sepharose column (16 mm × 20 cm; GE Healthcare) equilibrated in buffer A. A gradient from 200 mM NaCl to 1 M NaCl was used for elution (200 ml at a flow rate of 2.5 ml/min). This step was repeated twice. The recovered protein was loaded onto a Superdex 200 10/300 column (GE Healthcare) equilibrated in buffer A. The Sp-Cdc123 pool was concentrated to 10 mg/ml. Sp-Cdc123 behaves as a monomer in solution, as shown by SEC-MALS (Wyatt).

A truncated version of Sp-Cdc123 was engineered by introducing a stop codon in place of codon 275. The obtained plasmid, pET15b-SpCdc123Δc, produced a protein ending at residue 274 carrying a polyhistidine tag at the N-terminal extremity. pET15b-SpCdc123Δc was transformed into *E. coli* BL21 Rosetta and expression was obtained as described above. After sonication, the crude extract was loaded onto a column (4 ml) containing Talon affinity resin (Clontech) equilibrated in buffer B (10 mM HEPES [pH 7.5], 500 mM NaCl, 3 mM 2-mercaptoethanol, 0.1 mM PMSF, 0.1 mM benzamidine). The protein was eluted with buffer B containing 125 mM imidazole. The recovered protein was then loaded onto a Superdex 200 column (10/300; GE Healthcare) equilibrated in buffer B. The Sp-Cdc123Δc pool was concentrated to 10 mg/ml.

Sp-Cdc123:Sc-γDIII Complex

The gene coding for the γDIII domain (fragment 410–527) of Sc-eIF2 from PWS3915 (Perzlmaier et al., 2013) was cloned in pET3alpa. The obtained plasmid pET3a-Sc-γΔIII was transformed into *E. coli* BL21 Rosetta and expression was obtained as described above.

To purify the Sp-Cdc123:Sc-γDIII complex, pellets corresponding to 1 l of culture of BL21 Rosetta *E. coli* cells transformed with pET3a-Sc-γΔIII and 1 l of culture of BL21 Rosetta *E. coli* cells transformed with pET15b-Sp-Cdc123 were resuspended in buffer B (10 mM HEPES [pH 7.5], 500 mM NaCl, 3 mM 2-mercaptoethanol, 0.1 mM PMSF, 0.1 mM benzamidine) and mixed. After sonication, the crude extract was loaded onto a column (4 ml) containing Talon affinity resin (Clontech) equilibrated in buffer B. Finally, the protein complex was eluted with buffer B containing 125 mM imidazole. The recovered protein complex was finally loaded onto a Superdex 200 column (10/300; GE Healthcare) equilibrated in buffer B. Fractions containing Sp-Cdc123:Sc-γDIII were pooled and concentrated to 10 mg/ml (Figure S3B).

Crystallization and Structure Determinations

Sp-Cdc123

Initial crystallization trials were performed at 4°C and 24°C using sitting drops made with a Mosquito robot (TTP Labtech) and standard commercial kits (Hampton Research and Qiagen). Crystals were rapidly obtained using full-length Cdc123 in the presence of PEG 3350 as precipitating agent at 24°C (see detailed conditions in Table S1). Diffraction data were collected at 100 K (λ = 0.984 Å) on the Proxima-1 beamline at the SOLEIL synchrotron (Saint Aubin, France) equipped with a Pilatus detector. Data corresponding to crystals belonging to various space groups were collected (Table S1). These crystals diffracted to a maximum of 3.0 Å resolution. Diffraction images were analyzed with XDS (Kabsch, 1988), and the data were processed with programs of the CCP4 package (Collaborative Computational Project, Number 4, 1994).

Crystals were also obtained using the selenomethionylated version of full-length Cdc123. Highly redundant anomalous datasets were collected at 100 K at a wavelength corresponding to the maximal absorption of selenium (λ = 0.9792 Å). According to the weak diffraction pattern and the modest resolution limit of diffraction (around 4 Å), two datasets collected from Se-met crystals grown in the same drop were merged. A first experimental map was calculated at 5.5 Å resolution using the automated SAD phasing procedure of the Solve program within the PHENIX suite (Adams et al., 2010). A first round of automatic building was performed within this map using the "Phase and Build" function in Solve. The partial model allowed determination of the non-crystallographic symmetry operators. In a second step, a dataset corresponding to a crystal of full-length Cdc123 obtained in space group $P2_12_12_1$ was used to perform multiple crystal averaging (Table S1). The quality of the resulting map was clearly improved and allowed manual building of a first model in Coot (Emsley et al., 2010). During manual building, the Dali server was used to search for possible homologous structures. The crystal structure of the D-alanine:D-alanine ligase from *Bacillus anthracis* complexed with ATP (PDB: 3R5X) was identified and then used as a guide to facilitate further model building. In the course of refinement, the dataset corresponding to a crystal belonging to space group C222 was finally used to complete building of the model (Table S1). The preliminary structure of Cdc123 was partially refined to 3.24 Å resolution (R = 0.2689, R_{free} = 0.3079). This first model revealed that full-length Cdc123 was only partly defined in the electron density, with residues 274–319 being not visible. Therefore, to improve the quality of the crystals, a C-terminally truncated form of Cdc123 was engineered. Crystals obtained with the C-terminally truncated form of Cdc123 (Sp-Cdc123Δc) diffracted to 1.85 Å resolution (see detailed conditions in Table 1). New datasets were collected in the presence or absence of ATP or ATP analogs (Table 1). The 3.24-Å resolution model was used to solve the structures by molecular replacement using Phaser. The final structures of Cdc123Δc were refined to 1.85 and 2.06 Å resolution, in the presence or absence of ADP, respectively, using standard procedures in PHENIX. Final statistics are shown in Table 1.

Sp-Cdc123:Sc-eIF2γDIII Complex

The complex stored in buffer B was used for crystallization trials. Crystals were obtained in the presence of 25% PEG 3350 and 0.2 M $LiSO_4$ with or without ATP-Mg^{2+} (see detailed conditions in Table 1). Datasets were collected on the PX1 beamline at the SOLEIL synchrotron. The same procedure as described above was used to process the data. The structure was solved by molecular replacement with Phaser (Storoni et al., 2004), using the Cdc123Δc structure determined in this work and the γDIII domain from archaeal aIF2γ (PDB: 2AHO) as search models. The final structures were refined to 2.9 and 3.0 Å resolution in the presence or absence of ATP-Mg^{2+}, respectively (Table 1). According to the relatively modest resolution of the dataset as well as to the high B value of the structure, attribution of the sequence in the disconnected helix 275–296 remained tentative.

ACCESSION NUMBERS

Structure coordinates have been deposited in the PDB as follows. PDB: 4ZGO (Sp-Cdc123Δc), 4ZGP (Sp-Cdc123Δc:ADP), 4ZGN (Sp-Cdc123:Sc-γDIII:ATP), 4ZGQ (Sp-Cdc123:Sc-γDIII).

SUPPLEMENTAL INFORMATION

Supplemental Information includes Supplemental Experimental Procedures, six figures, and one table and can be found with this article online at http://dx.doi.org/10.1016/j.str.2015.06.014.

AUTHOR CONTRIBUTIONS

E.S., W.S., and Y.M. designed the research. M.P., E.D., L.A., J.P., E.S., and Y.M. performed the experiments. E.S., W.S., and Y.M. wrote the paper, and all authors revised the manuscript.

ACKNOWLEDGMENTS

This work was supported by grants from the Center National de la Recherche Scientifique and by Ecole polytechnique to Unité Mixte de Recherche no. 7654. E.D. was a recipient of a Gaspard Monge PhD fellowship from Ecole polytechnique. We thank the staff of the macromolecular crystallography beamlines at the SOLEIL synchrotron (Saint-Aubin, France), and in particular Pierre Legrand, for expert assistance during data collection and Andrea Brücher, Antje Machetanz-Morokane, and Adelheid Weissgerber for their expert technical assistance with the yeast work. We thank François Lacroute (Institut National de la Recherche Agronomique, Grignon, France) for the generous gift of the *S. pombe* cDNA library.

Received: May 13, 2015
Revised: June 16, 2015
Accepted: June 18, 2015
Published: July 23, 2015

REFERENCES

Adams, P.D., Afonine, P.V., Bunkóczi, G., Chen, V.B., Davis, I.W., Echols, N., Headd, J.J., Hung, L.-W., Kapral, G.J., Grosse-Kunstleve, R.W., et al. (2010). PHENIX: a comprehensive Python-based system for macromolecular structure solution. Acta Crystallogr. D Biol. Crystallogr. *66*, 213–221.

Adelaide, J., Finetti, P., Bekhouche, I., Repellini, L., Geneix, J., Sircoulomb, F., Charafe-Jauffret, E., Cervera, N., Desplans, J., Parzy, D., et al. (2007). Integrated profiling of basal and luminal breast cancers. Cancer Res. *67*, 11565–11575.

Algire, M.A., Maag, D., and Lorsch, J.R. (2005). Pi release from eIF2, not GTP hydrolysis, is the step controlled by start-site selection during eukaryotic translation initiation. Mol. Cell *20*, 251–262.

Artymiuk, P.J., Poirrette, A.R., Rice, D.W., and Willett, P. (1996). Biotin carboxylase comes into the fold. Nat. Struct. Biol. *3*, 128–132.

Cole, C., Barber, J., and Barton, G. (2008). The Jpred 3 secondary structure prediction server. Nucleic Acids Res. *35*, W197–W201.

Collaborative Computational Project, Number 4 (1994). The CCP4 suite: programs from protein crystallography. Acta Crystallogr. D Biol. Crystallogr. *50*, 760–763.

Dubiez, E., Aleksandrov, A., Lazennec-Schurdevin, C., Mechulam, Y., and Schmitt, E. (2015). Identification of a second GTP-bound magnesium ion in archaeal initiation factor 2. Nucleic Acids Res. *43*, 2946–2957.

Emsley, P., Lohkamp, B., Scott, W.G., and Cowtan, K. (2010). Features and development of Coot. Acta Crystallogr. D Biol. Crystallogr. *66*, 486–501.

Fan, C., Moews, P.C., Shi, Y., Walsh, C.T., and Knox, J.R. (1995). A common fold for peptide synthetases cleaving ATP to ADP: glutathione synthetase and D-alanine:D-alanine ligase of *Escherichia coli*. Proc. Natl. Acad. Sci. USA *92*, 1172–1176.

Fawaz, M.V., Topper, M.E., and Firestine, S.M. (2011). The ATP-grasp enzymes. Bioorg. Chem. *39*, 185–191.

Galperin, M.Y., and Koonin, E.V. (1997). A diverse superfamily of enzymes with ATP-dependent carboxylate-amine/thiol ligase activity. Protein Sci. *6*, 2639–2643.

Gebauer, F., and Hentze, M.W. (2004). Molecular mechanisms of translational control. Nat. Rev. Mol. Cell Biol. *5*, 827–835.

Hara, T., Kato, H., Katsube, Y., and Oda, J. (1996). A pseudo-Michaelis quaternary complex in the reverse reaction of a ligase: structure of *Escherichia coli* B glutathione synthetase complexed with ADP, glutathione, and sulfate at 2.0 A resolution. Biochemistry *35*, 11967–11974.

Hinnebusch, A.G. (2005). Translational regulation of GCN4 and the general amino acid control of yeast. Annu. Rev. Microbiol. *59*, 407–450.

Hinnebusch, A.G. (2011). Molecular mechanism of scanning and start codon selection in eukaryotes. Microbiol. Mol. Biol. Rev. *75*, 434–467.

Ho, Y., Gruhler, A., Heilbut, A., Bader, G.D., Moore, L., Adams, S.L., Millar, A., Taylor, P., Bennett, K., Boutilier, K., et al. (2002). Systematic identification of protein complexes in *Saccharomyces cerevisiae* by mass spectrometry. Nature *415*, 180–183.

Holcik, M., and Sonenberg, N. (2005). Translational control in stress and apoptosis. Nat. Rev. Mol. Cell Biol. *6*, 318–327.

Holm, L., and Sander, C. (1995). Dali: a network tool for protein structure comparison. Trends Biochem. Sci. *20*, 478–480.

Huang, H.K., Yoon, H., Hannig, E.M., and Donahue, T.F. (1997). GTP hydrolysis controls stringent selection of the AUG start codon during translation initiation in *Saccharomyces cerevisiae*. Genes Dev. *11*, 2396–2413.

Kabsch, W.J. (1988). Evaluation of single crystal X-ray diffraction data from a position sensitive detector. J. Appl. Crystallogr. *21*, 916–924.

Laskowski, R.A., Mac Arthur, M.W., Moss, D.S., and Thornton, J.M. (1993). PROCHECK: a program to check the stereochemical quality of protein structure. J. Appl. Crystallogr. *26*, 283–291.

Liu, S., Chang, J.S., Herberg, J.T., Horng, M.M., Tomich, P.K., Lin, A.H., and Marotti, K.R. (2006). Allosteric inhibition of *Staphylococcus aureus* D-alanine:D-alanine ligase revealed by crystallographic studies. Proc. Natl. Acad. Sci. USA *103*, 15178–15183.

Lorsch, J., and Dever, T. (2010). Molecular view of 43S complex formation and start site selection in eukaryotic translation initiation. J. Biol. Chem. *285*, 21203–21207.

Miller, G.J., Wilson, M.P., Majerus, P.W., and Hurley, J.H. (2005). Specificity determinants in inositol polyphosphate synthesis: crystal structure of inositol 1,3,4-trisphosphate 5/6-kinase. Mol. Cell *18*, 201–212.

Naveau, M., Lazennec-Schurdevin, C., Panvert, M., Dubiez, E., Mechulam, Y., and Schmitt, E. (2013). Roles of yeast eIF2alpha and eIF2beta subunits in the binding of the initiator methionyl-tRNA. Nucleic Acids Res. *41*, 1047–1057.

Ohno, K., Okuda, A., Ohtsu, M., and Kimura, G. (1984). Genetic analysis of control of proliferation in fibroblastic cells in culture. I. Isolation and characterization of mutants temperature-sensitive for proliferation or survival of untransformed diploid rat cell line 3Y1. Somatic Cell Mol. Genet. *10*, 17–28.

Okuda, A., and Kimura, G. (1996). An amino acid change in novel protein D123 is responsible for temperature-sensitive G1-phase arrest in a mutant of rat fibroblast line 3Y1. Exp. Cell Res. *223*, 242–249.

Pedulla, N., Palermo, R., Hasenohrl, D., Blasi, U., Cammarano, P., and Londei, P. (2005). The archaeal eIF2 homologue: functional properties of an ancient translation initiation factor. Nucleic Acids Res. *33*, 1804–1812, Print 2005.

Perzlmaier, A.F., Richter, F., and Seufert, W. (2013). Translation initiation requires cell division cycle 123 (Cdc123) to facilitate biogenesis of the eukaryotic initiation factor 2 (eIF2). J. Biol. Chem. *288*, 21537–21546.

Roll-Mecak, A., Alone, P., Cao, C., Dever, T.E., and Burley, S.K. (2004). X-ray structure of translation initiation factor eIF2gamma: implications for tRNA and eIF2alpha binding. J. Biol. Chem. *279*, 10634–10642.

Roper, D.I., Huyton, T., Vagin, A., and Dodson, G. (2000). The molecular basis of vancomycin resistance in clinically relevant Enterococci: crystal structure of D-alanyl-D-lactate ligase (VanA). Proc. Natl. Acad. Sci. USA *97*, 8921–8925.

Schmitt, E., Blanquet, S., and Mechulam, Y. (2002). The large subunit of initiation factor aIF2 is a close structural homologue of elongation factors. EMBO J. *21*, 1821–1832.

Schmitt, E., Naveau, M., and Mechulam, Y. (2010). Eukaryotic and archaeal translation initiation factor 2: a heterotrimeric tRNA carrier. FEBS Lett. *584*, 405–412.

Schmitt, E., Panvert, M., Lazennec-Schurdevin, C., Coureux, P.D., Perez, J., Thompson, A., and Mechulam, Y. (2012). Structure of the ternary initiation complex aIF2-GDPNP-methionylated initiator tRNA. Nat. Struct. Mol. Biol. *19*, 450–454.

Schrodinger, LLC. (2010). The PyMOL Molecular Graphics System, Version 1.3r1 (Schrodinger, LLC).

Sloane, V., Blanchard, C.Z., Guillot, F., and Waldrop, G.L. (2001). Site-directed mutagenesis of ATP binding residues of biotin carboxylase. Insight into the mechanism of catalysis. J. Biol. Chem. *276*, 24991–24996.

Soler Artigas, M., Loth, D.W., Wain, L.V., Gharib, S.A., Obeidat, M., Tang, W., Zhai, G., Zhao, J.H., Smith, A.V., Huffman, J.E., et al. (2011). Genome-wide association and large-scale follow up identifies 16 new loci influencing lung function. Nat. Genet. *43*, 1082–1090.

Stolboushkina, E., Nikonov, S., Nikulin, A., Blasi, U., Manstein, D.J., Fedorov, R., Garber, M., and Nikonov, O. (2008). Crystal structure of the intact archaeal translation initiation factor 2 demonstrates very high conformational flexibility in the alpha- and beta-subunits. J. Mol. Biol. *382*, 680–691.

Storoni, L.C., McCoy, A.J., and Read, R.J. (2004). Likelihood-enhanced fast rotation functions. Acta Crystallogr. D Biol. Crystallogr. *60*, 432–438.

Yatime, L., Schmitt, E., Blanquet, S., and Mechulam, Y. (2004). Functional molecular mapping of archaeal translation initiation factor 2. J. Biol. Chem. *279*, 15984–15993.

Yatime, L., Mechulam, Y., Blanquet, S., and Schmitt, E. (2006). Structural switch of the gamma subunit in an archaeal aIF2 alpha gamma heterodimer. Structure *14*, 119–128.

Yatime, L., Mechulam, Y., Blanquet, S., and Schmitt, E. (2007). Structure of an archaeal heterotrimeric initiation factor 2 reveals a nucleotide state between the GTP and the GDP states. Proc. Natl. Acad. Sci. USA *104*, 18445–18450.

Zeggini, E., Scott, L.J., Saxena, R., Voight, B.F., Marchini, J.L., Hu, T., de Bakker, P.I., Abecasis, G.R., Almgren, P., Andersen, G., et al. (2008). Meta-analysis of genome-wide association data and large-scale replication identifies additional susceptibility loci for type 2 diabetes. Nat. Genet. *40*, 638–645.

Zhao, G., Jin, Z., Wang, Y., Allewell, N.M., Tuchman, M., and Shi, D. (2013). Structure and function of *Escherichia coli* RimK, an ATP-grasp fold, L-glutamyl ligase enzyme. Proteins *81*, 1847–1854.

